International Forum on Aeroelasticity and Structural Dynamics
IFASD 2017
25-28 June 2017 Como, Italy

INCLUSION OF PROPELLER EFFECTS ON AEROELASTIC BEHAVIOR OF VERY FLEXIBLE AIRCRAFT

Patrícia C. Teixeira[1] **and Carlos E. S. Cesnik**[1]

[1]Department of Aerospace Engineering
University of Michigan
1320 Beal Avenue, Ann Arbor, MI 48109 USA
pct@umich.edu
cesnik@umich.edu

Keywords: aerodynamic propeller effects, very flexible wing, particle vortex aerodynamics

Abstract: Although propeller propulsion is present in many high-altitude long-endurance aircraft (e.g., Aerovironments Helios, University of Michigan's X-HALE UAS, etc.), the effect of the propeller slipstream on the aeroelastic behavior of such vehicles for coupled nonlinear aeroelastic-flight mechanics simulation is generally not taken into account. On the other hand, one important feature desired for aeroelastic tools is the capability of providing accurate results with small computational cost, eventually enabling real-time simulations.

This work presents an enhancement to an existing aeroelastic framework that enables the investigation of propeller effects on very flexible aircraft. This is achieved by coupling a geometrically non-linear aeroelastic structural solver with an Unsteady Vortex Lattice code capable of dealing with high structural displacements for the aircraft lifting surfaces and a Lifting Line/Viscous Vortex Particle Method for the propeller effects and applying the enhanced framework to investigate the interference between a flexible wing and a propeller.

1 INTRODUCTION

There are some studies in the literature dealing with the investigation of aerodynamic wing-propeller interference in general, however very few can be found when this is applied to aeroelastic problems. Examples of such can be found in the experimental work of Gamble and Reeder [1] and the numerical work of Agostinelli *et al.* [2].

Gamble and Reeder [1] studied the influence of propeller on a flexible wing micro-air-vehicle (MAV) and has found that the relative position between the propeller and the wing influence pitch and yaw stability. A numerical work was performed by Agostinelli *et al.* [2]. The approach was proposed for conceptual design. The aerodynamic model consisted of a pre-determined database of CFD or experimental data coupled with lifting-line theory to estimate propeller slipstream effects along the wing span. The aerodynamic forces were integrated with a beam finite element model, with a linear relation between forces and displacements. The study focused on the effects of propeller on the lift coefficient along the spanwise direction and no dynamic simulation was performed.

The absence of a propeller model is a potential source of error for aeroelastic simulations. In Jones and Cesnik [3], correlations between the X-HALE experimental and numerical results

using the UM/NAST solver [4–6] is presented. It was observed, for example, that for a condition where the simulations predicted high amplitudes for roll and pitch, the observed in the flight test was just a soft Dutch-roll-like behavior, which was damped out in two cycles without pilot intervention. As discussed in [3], there are many possible reasons that may explain the differences noticed including the missing propeller aerodynamic effects.

In Veldhuis [7] and Calabretta [8], investigations of the interference between propeller and wing were performed (although not focused on very flexible wings). In [7], the influence of propellers position on aerodynamic performance was investigated. Models of varying complexities were used for the propeller-wing combination: empirical momentum theory, Vortex Lattice Method (VLM) coupled with blade-element propeller model, Panel Method (PM) with a slipstream envelop model and RANS simulations. A swirl recovery factor (SRF) was considered for the VLM method to consider the reduction of the propeller slipstream velocity due to the presence of the wing. For that model, the influence of both the propeller on the wing and the wing on the propeller were considered. This coupling was usually neglected by previous works.

In [8], a simplified model for propeller/airframe interaction was proposed to be used in optimization studies of early design stages of aircraft with propeller. The approach was a combination of PM for the airframe and actuator disk (a pseudo-steady model) and Vortex Particle to model the propeller and the propeller wake, respectively. The lack of connectivity among particles in the Vortex Particle (VP) method and the use of a not completely steady approach allowed the propeller wake to flow in a more natural way then in other previous propeller/airframe simplified approaches. Other examples along those lines can be found in the works of Puneet and Friedmann [9], Thepvongs *et al.* [10], and He and Zhao [11] where the authors use VP to model propeller or rotor slip stream. Particularly, the work of [11] uses Lifting Line and Viscous Particle Vortex to model the dynamics of a rotor. As pointed out by Willis [12] and He and Zhao [11], the main advantages of using VP for wake modeling are: i) Lagrangian formulation, implying no need for mesh generation; ii) no connectivity between particles, allowing automatic, hands off wake evolution in more complex environments; iii) possibility of including viscous effects in the diffusion of vorticity without the problem of artificial numerical dissipation as in CFD; iv) no need of previous determination of wake position and wake-body intersections. The VP method needs to be coupled with some other method to model bound vorticity at lifting surfaces, as the particles are generated based on the vorticity released into the wake. There are many possibilities of methods for that, as CFD, Panel Method, Actuator Disk, etc.

This paper presents an approach to include propeller slipstream effects on a coupled aeroelastic-flight mechanics framework in order to investigate its influence on static and dynamic simulations of very flexible aircraft. It is based on a Lifting Line method for the propeller blades and a Viscous Vortex Particle Method (VVPM) for the propeller wake. They were coupled with an unsteady VLM (uVLM) and a geometrically non-linear composite beam models for the airframe. In this work Lifting Line Method was chosen for its simplicity, small computational cost and good capability to represent the unsteady behavior of the blade circulation [13].

2 THEORETICAL FORMULATION

This section describes the theoretical formulations employed in this study, along with their integration into a geometrically-nonlinear aeroeastic-flight dynamics coupled framework. It includes a short description of the original University of Michigan‘s Nonlinear Aeroelastic Sim-

ulation Toolbox (UM/NAST), followed by the various aerodynamic pieces and their integration into this new framework.

2.1 New enhanced aeroelastic framework to account for aerodynamic propeller effects.

In this work the University of Michigan's Nonlinear Aeroelastic Simulation Toolbox (UM/NAST) [4–6] is coupled to an Unsteady Vortex Lattice (uVLM) code developed in Ritter *et al.* [14] to model the aerodynamics of the aircraft lifting surfaces, and a Lifting Line and VP models for the propellers. The structural formulation employs a strain-based finite element and the slender aircraft members are represented by beams. As uVLM needs a 3D grid to represent the surfaces, an interface between the structural and aerodynamic solvers is necessary in order to transfer loads and displacements between those solvers.

The new aeroelastic framework for the coupled structural/aerodynamic models is shown in Fig. (1). Based on the current applied loads and control inputs the structural solver determines the new coordinates of the beam. Those coordinates are converted into a panel grid for the uVLM solver. Then, based on the current geometry, circulation of propeller blades and distribution of vortex particles, the new circulation and loads at the panels are calculated. After that, based on the updated circulation of panels and wake panels, the circulation of propeller blades segments and new distribution of propeller wake vortex particles (new positions and associated vorticity) are calculated for the next step. In next sections more details will be provided about each solver formulation and how they are integrated.

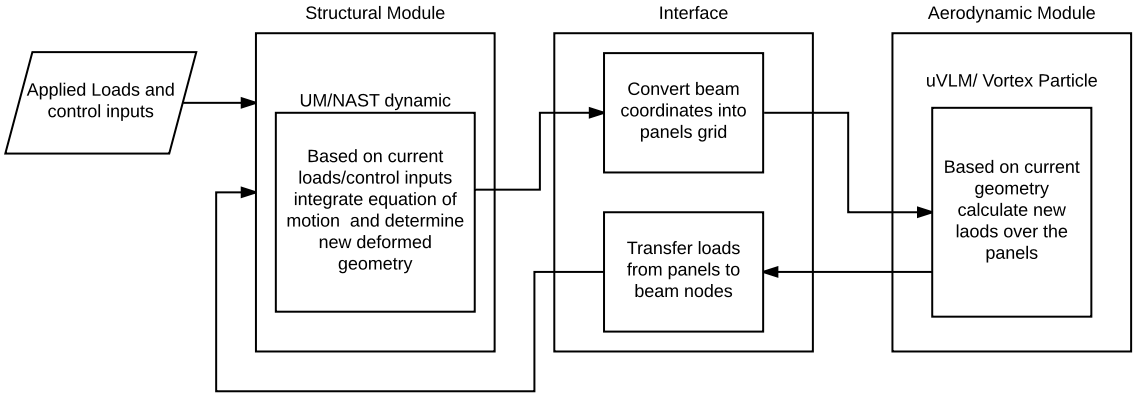

Figure 1: Aeroelastic framework.

2.2 Geometrically-nonlinear Structural Model: Strain-based Finite Element

The structural model formulation in UM/NAST considers non-linear equations of motion using a low-order strain-based nonlinear structural element model [4]. The structure is modeled as beams discretized by elements with constant strain in extension, twist, and in/out-of-plane bending. Those strain values are then converted to a vector position that contains the coordinates and local orientation at each point along the beam. A detailed description about UM/NAST structural formulation can be found in [15]

2.3 Aerodynamic Model of Lifting Surfaces: Unsteady Vortex Lattice

The UM/NAST solver originally employed a corrected strip theory to calculate the unsteady aerodynamic loads. However, to include the presence of propellers, a method that allows to take into account the influence between lifting surfaces was necessary. Unsteady Vortex Lattice is a suitable method for this purpose. It enables one to account for the induced velocity due to different sources, like the induced velocities due to each panel, panel wake, and influence of the propeller blade and slipstream induced velocity. Also, as described in [14], the uVLM solver considers translation and rotation of the panels due to arbitrary elastic deformations - allowing simulations with large structural displacements - and has a smaller computational cost compared to unsteady RANS solutions.

Then, for the purpose described above, an Unsteady Vortex Lattice code developed by Ritter *et al.* [14] was coupled to UM/NAST. The method assumes potential flow formulation and employs vortex ring elements distributed along wing panels and wake. The circulation is calculated such that zero normal velocity at each panel control point is satisfied, taking into account the normal components of free stream and induced velocity due to panels, wake and any other sources.

The lifting members are modeled as cambered surfaces (surfaces composed by each airfoil camber line). A wake-stepping method is used for the wake that is convected with the onflow velocity. Influence of panels, wake, and other sources can also be included, but the computational cost may increase and problems due to wake roll up may appear. Therefore, for simplicity in the present implementation, the wake is convected with just onflow velocity.

2.4 Structural and Aerodynamic Model Integration

As the structural model employs a 1D finite element model, while the uVLM uses 3D grid, an interface between the two solvers is necessary, calculating wing panels based on current beam geometry and transferring panel loads to beam structural nodes. The transfer of forces from panels to beams is accomplished in two steps:

i) Energy-consistent transfer of loads from the panels to the points along the beam given by panel discretization:

Assuming negligible deformations in chordwise direction, the displacements of each panel quarter point (points located at 1/4 of panel chord from panel leading edge and half panel span) can be written as a function of the points given by spanwise discretization along the beam. Then, in order to have the virtual work provided by the distribution of generalized forces on aerodynamic grid points equivalent to the virtual work performed by the distribution of generalized forces over the beam nodes, one has:

$$\{\delta u_a\}^T \{F_a\} = \{\delta u_s\}^T \{F_s\} \tag{1}$$

where $\{F_a\}$ and $\{F_s\}$ are column vectors containing the generalized aerodynamic and structural forces on each point (over the aerodynamic grid and structural nodes, respectively), and $\{\delta u_a\}$ and $\{\delta u_s\}$ are the corresponding virtual displacements. Then, as the displacements of the

quarter-chord points and nodes along the beam are related by the assumption of a rigid chord-wise direction, an energy-consistent relation to transfer forces from panels to beam nodes can be determined.

ii) linear transfer of loads from those points to the structural nodes:

The loads at beam nodes given by span-wise discretization may need to be transfered to the structural nodes, as aerodynamic and structural span-wise discretizations can be different. For this case, a linear approach to transfer loads to neighboring structural nodes is employed. As UM/NAST formulation considers elements with constant curvature, the linear transfer of moments is coherent with that assumption.

The calculation of aerodynamic grid based on structural nodes also considers the assumption of rigid chord-wise direction. In this case, for each section, the airfoil camber coordinates are re-written from the airfoil frame to body frame based on a transformation matrix associated with coordinate systems defined in UM/NAST, which considers a body system, a local system related with the orientation of each section and an airfoil coordinate system in the case of swept wings.

2.5 Propeller Model

2.5.1 Propeller Blade Model: Lifting Line

The propeller blades are represented as a line passing through the 1/4-chord location from leading edge at each aifoil section. The blades are discretized in N segments with the assumption of constant circulation in each one. For each section the angle with respect to the plane of rotation, airfoil type and associated polar table need to be provided. Control points are defined in the middle of each segment where the circulation is calculated based on the local effective angle of attack and Reynolds number. The grid defining the blade segments is updated for the current time step by:

$$y = y_H + rcos(\Omega t + \theta_0) \tag{2}$$

$$z = z_H + rsin(\Omega t + \theta_0) \tag{3}$$

where y and z are coordinates defining the plane of rotation of the lifting line, the subscript H represents the propeller hub coordinates, Ω is the angular propeller velocity and θ_0 is the initial angular blade position (just a reference value to determine the blade angular position) and r is the radial position of each point. The values of hub coordinates are updated at each time step by the new values calculated in the structural solver.

For the initial time no wake is present and c_l and c_d are determined from polar tables considering geometric angle of attack (if there is just an isolated propeller) or the effective angle of attack taking into account the induced velocities due to other sources. For the next time steps, the induced velocity due to the various particles are also included.

Then, based on c_l, the circulation is calculated from:

$$\Gamma = 1/2 c V_{section} c_l \tag{4}$$

where Γ is the circulation at the considered control point, c is the local chord, $V_{section}$ is the component of total velocity at the control point that is in the plane of airfoil section considered, and c_l is the local lift coefficient. This equation comes from a combination of 2D Kutta-Jukowski theory and the definition of lift coefficient.

Based on the updated values of circulation, new particles are generated by the formulation described in the next section. Also, with drag, c_d, and lift, c_l, coefficients at each section control points, the loads acting on the propeller hub can be calculated.

2.5.2 Propeller Wake Model: Viscous Vortex Particle

The Viscous Vortex Particle method is based on the Lagrangian format of the vorticity-velocity equation of incompressible flow, ***i.e.***,

$$D\vec{\omega}/dt = \vec{\omega}.\nabla\vec{u} + \nu\nabla^2\vec{\omega} \tag{5}$$

where $\vec{\omega}$ is the vorticity field, $\vec{u}$ is the associated velocity field, and ν is the kinematic viscosity.

A vortex particle can be interpreted as a physical singularity influencing all the flow field similarly as source and doublet singularities [8]. The vorticity field is then discretized in those particles and can be written as the summation of the contribution of each particle vorticity field:

$$\vec{\omega}(\vec{x},t) = \sum_{i=1}^{n_p} \epsilon_\sigma(\vec{x}-\vec{x_i})\vec{\alpha_i} = \sum_{i=1}^{n_p} \epsilon_\sigma(\vec{x}-\vec{x_i})\vec{\omega_i}vol_i \tag{6}$$

where $\vec{x_i}$ and $\vec{\alpha_i}$ are the position and strength (with unit of vorticity per unit of volume) associated with particle i, respectively. ϵ is a distribution function associated to the particle vorticity field and ϵ_σ is defined as $\epsilon_\sigma = \epsilon/\sigma^3$. In this work, a Gaussian distribution for σ is used as done by [9, 11]. Others possibilities of distribution functions can be found in [16]. σ is a smoothing parameter of the method and for convergence it should be as minimum as possible, but greater than the minimum typical distance between two particles (core overlapping condition) [16], [11].

Based on Eq. (5) and Eq. (6), the following governing equations to update particles positions and strength can be derived (details can be found in [16]):

$$D\vec{\alpha}/Dt = \vec{\alpha}.\nabla\vec{u} + \nu\nabla^2\vec{\alpha} \tag{7}$$

$$\vec{u} = -\sum_{i=1}^{n_p} 1/\sigma_i^3 K(\rho)(\vec{x}-\vec{x_i}) \times \alpha_i \tag{8}$$

where $\rho = |\vec{x}-\vec{x_i}|/\sigma_i$ is a nondimensional distance parameters and $K(\rho)$ is the Biot-Sarvat kernel.

After each time step, new particles are generated satisfying the conservation of vorticity. Then, the spatial and temporal variation of vorticity in each blade segment corresponds to the generation of new vorticity released into the wake, called trailing and shed vorticities, respectively. In this work, where Lifting Line is used to model the blades, the shed particles strength from each segment is calculated as:

$$\vec{\alpha}_{shed} = (d\vec{\Gamma}_b/dt)\ dt\ s_b \tag{9}$$

where $\vec{\Gamma}_b$ is the circulation at a given blade segment, dt is the size of time step, and s_b is the length of the considered blade segment (as shed particles represent vortex filaments released aligned with blade segment). The positions of new shed particles are located in the centroid of the area that each blade segment travels with velocity $\vec{v_b}$ in one time step, where $\vec{v_b}$ in the velocity of the blade with relation to the flow (due to onflow velocity, propeller rotation and other possible sources).

The trailing particle strength is related to the spatial change of circulation from one segment to the next and it represents vortex filaments of size $|vecv_b\ dt|$ in the direction of local flow velocity as:

$$\vec{\alpha}_{trailing} = (\Gamma_{i-1} - \Gamma_i)\ \vec{v_b}\ dt \tag{10}$$

where Γ_i and Γ_{i-1} are the scalar values of circulations at adjacent blade segments $i-1$ and i with i increasing from root to tip (for tip it means tip circulation minus zero), and $\vec{v_b}$ is the blade velocity with respect to the flow. In similar way as for shed particles, the position of new trailing particles are located in the middle of the line given by $vecv_b\ dt$, representing the line traveled by each grid points in one time step. The direction of the trailing particle at tip should be such that the induced velocity created by a released trailing particle is along the opposite direction of thrust. Then, depending on what is the direction of rotation of propeller that generates positive thrust, the strength direction at tip may have the same or opposite direction to the local flow velocity.

A drawback of Vortex Particle formulation is that for N particles it has a characteristic speed of $O(N^2)$. Then, as the number of particles increase with time, the computational cost increases significantly and some acceleration procedure may be necessary. In this work a cut-off distance is applied when particles are far away from the region of interest.

More details about Viscous Vortex Particle formulation can be found in [11, 16].

2.5.3 Propeller and Unsteady Vortex Lattice Integration

For the integration of the propeller and the uVLM solvers, the influence of the propeller vortex particles and propeller bound vorticity into the airframe surface panels, and the influence of airframe surface panels and wake panels on the slipstream particles and on the blade bound vorticity (influencing blades effective angles and the distribution of circulation) are taken into account as described here. At a given time step, the panels' and wake panels' circulations are updated by uVLM considering current geometry, current particle distribution (calculated during previous time), and induced velocities (including propellers). Then, based on the new panels'

and wake panels' circulation, the new circulation of the blades are calculated, the existing particles have positions and strength updated, and new particles are generated, defining new particle distribution for next time step. As it is important to have a time step dt smaller then the propeller period, one should consider the dt of the propeller smaller than the dt of the global dynamic solver. In this work it was considered the dt of the propeller half of the dt of the dynamic solver.

3 NUMERICAL RESULTS

This section summarizes the numerical studies based on the new formulation described above. Cases are used for verification of the implementation and for some preliminary investigations of the propeller effects.

Several assumptions were made for the numerical cases presented here that are listed next. In the structural model a trapezoidal method was employed to integrate the equations of motion, a damping of 0.03 and a time step of 0.002 were considered (with a sub-time step of 0.001 for the propellers). As the Unsteady Vortex Lattice does not account by viscous drag the thrust generated by the propellers were not included in the structural calculations, avoiding unphysical behavior due to absence of viscous drag. The particle vortex formulation is used such that, at each time step, it generates just one trailing particle at each blade tip: as the circulation gradient is stronger there, it has a dominant effect on vorticity field and provides similar results as in the case of all blade segments included, saving computational cost. Also, for this case, shed particles have much smaller strength than trailing particles and can be removed without penalty in the results. The value of σ was chosen as 1.1 times the length of the arc traveled by the blade tip in one time step. The dynamic viscosity is $\mu = 1.7855\ 10^5$ N.s/m^2 and air density $\rho = 1.225$ kg/m^3.

For all simulation a model based on APC 11x5.5 thin-electric propeller was considered, with geometrical data described in [17]. Due to the lack of information about airfoil type along the blades, a constant typical APC airfoil was considered. It was employed an RPM of 6000 and a propeller time step corresponding to 10 steps per revolution.

3.1 Verification Cases

Before showing the numerical case studies for a rigid and elastic aircraft models, comparisons are first presented to verify the integration of the UM/NAST with the uVLM and the Viscous Vortex Particle formulations.

To verify the implementation of the Viscous Vortex Particle formulation, the comparison was done with results produced with a Viscous Vortex Particle code developed by [9]. For that the thrust coefficient (CT) produced by a simple one bladed propeller with data described in Table (1) was compared for a range of velocities between 0 and 30 m/s. As one can see from Fig. (2), the values of CT show a good agreement between the two implementations, with small deviations growing with increase in speed. The agreement is better in the region of positive thrust coefficient, which may be related to the fact that for negative CT the propeller is in the windmilling state.

To verify the integration between UM/NAST and uVLM, static aeroelastic results using NASTRAN coupled with the same uVLM code [18] were compared. The University of Michigan's X-HALE UAS was used as an example of a very flexible aircraft [19]. This vehicle was

Radius	0.15 m
Offset between hub and begin of blade	0.02 m
Angle of blade with plane of rotation	10 degrees
airfoil type	flat plate
Propeller RPM	6000
chord	0.01 m

Table 1: Propeller parameters for verification studies.

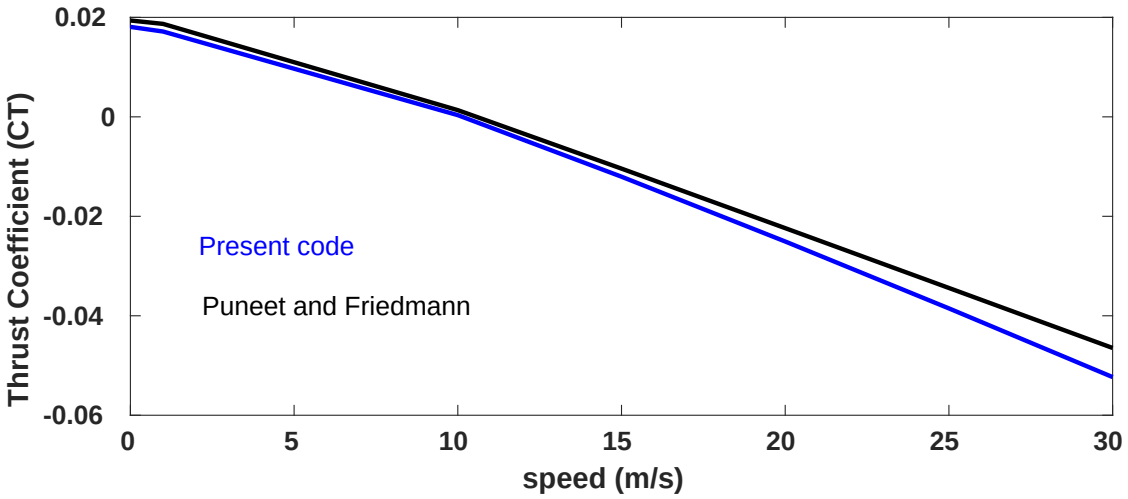

Figure 2: Comparison of results for Thrust Coefficient calculated with the present code and the code developed by Puneet and Friedmann [9].

conceived to collect experimental data for validation of nonlinear aeroelastic-coupled-flight-mechanics solvers. The vehicle has a wingspan of 6 m with a 0.2-m chord, five pods along the wing, five tails, three fins and five electric motor-propeller combinations located in front of each pod at spanwise locations $y = -2, -1, 0, 1$, and 2 meters, respectively. For the simulations, the propellers were located 20 cm ahead and 2 cm below of the wing leading edge, with a pitch angle of 5 degree between the propeller axis and the X-HALE wing, as the wing has an incidence angle with respect to the pods of 5 degrees. Figure (3) shows the basic aircraft geometry.

Figure (4) presents results for the X-HALE at a uniform flow velocity of 16 m/s and body angles of attack of 0, 0.5 and 1 degree. Solutions were obtained for two different solvers, that is, the new UM/NAST-uVLM and the NASTRAN (SOL400)-uVLM [18] codes. The results show excellent agreement, with slight differences that increase with angle of attack. The differences may be explained due to difference in the techniques used to transfer loads and displacements between the structural and aerodynamic solvers.

The coupling between the propeller model and the Unsteady Vortex Lattice was evaluated with respect to its expected qualitative behavior. As discussed above, the trailing particle strength vector is parallel to the local flow velocity and is such that the axial velocity its induces has opposite direction to the generated thrust. Considering the propeller frame described in Fig. (5) and a propeller with a twist such that a clockwise blade rotation with respect to the x-axis generates thrust in the $-x$ direction, one can see that trailing particles have approximately

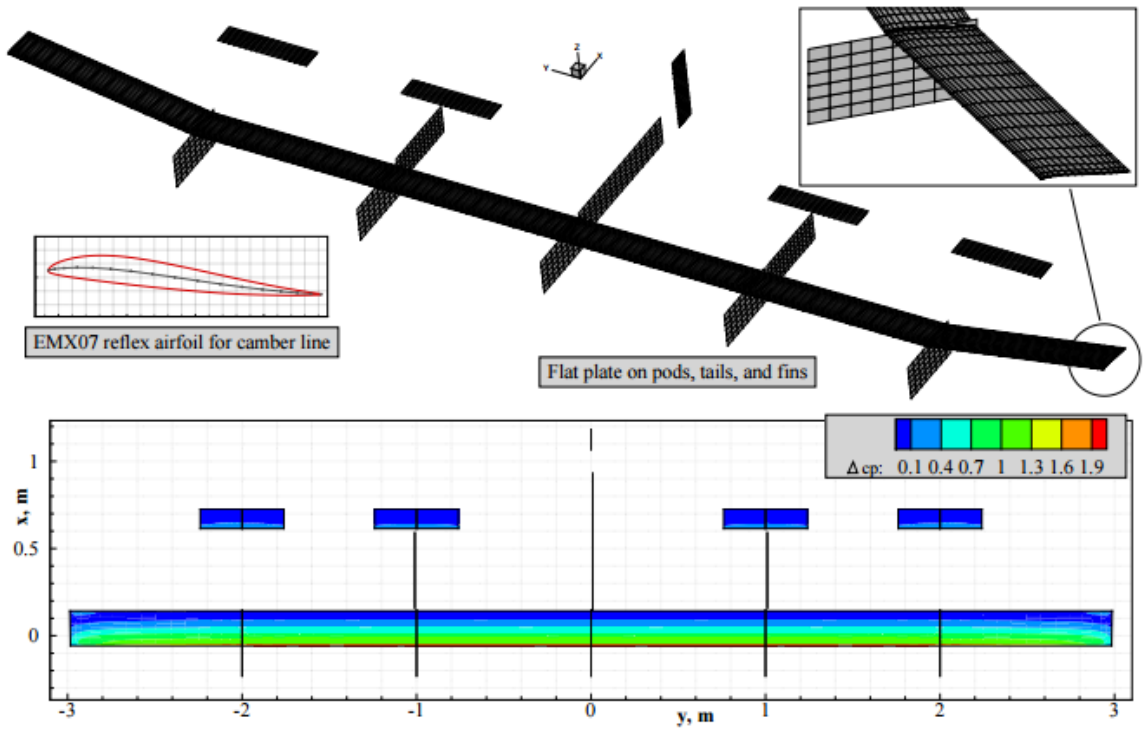

Figure 3: X-HALE model used for present studies. Source: [20].

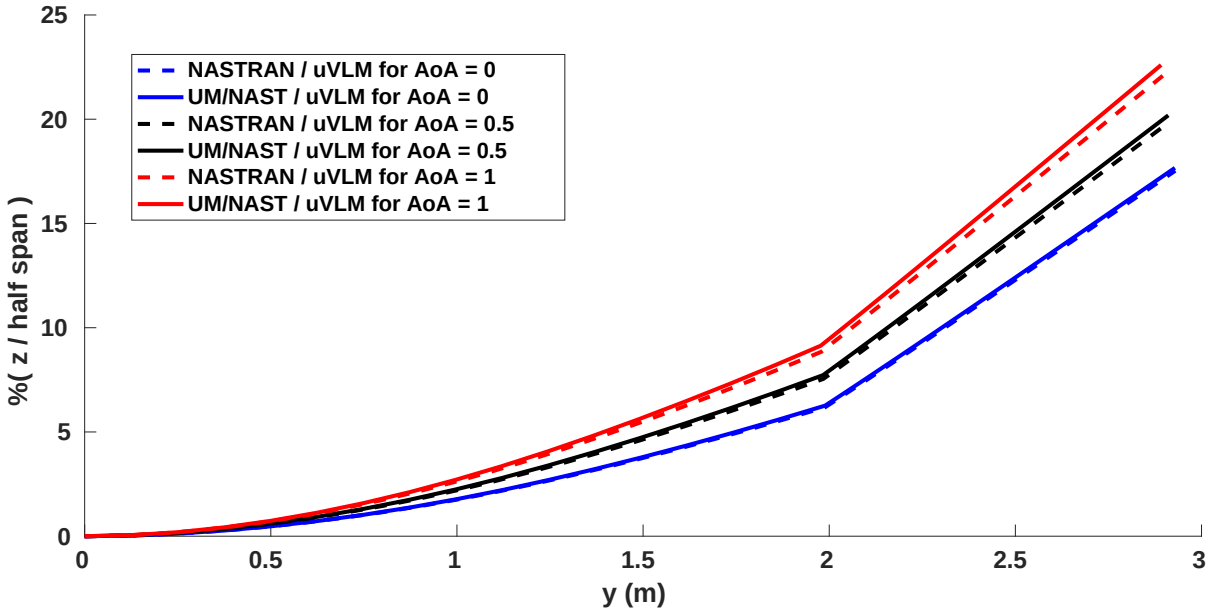

Figure 4: Right wing deformed configuration in the y-z plane.

the same direction (without considering the induced velocities) and sign as the effective flow velocity, given by the onflow velocity plus the velocity of the fluid with relation to the blade (due to blade rotation), generating an axial velocity opposite to thrust. Now, consider a wing placed on the $x-y$-plane and the incoming flow along the x direction (going towards negative x). By

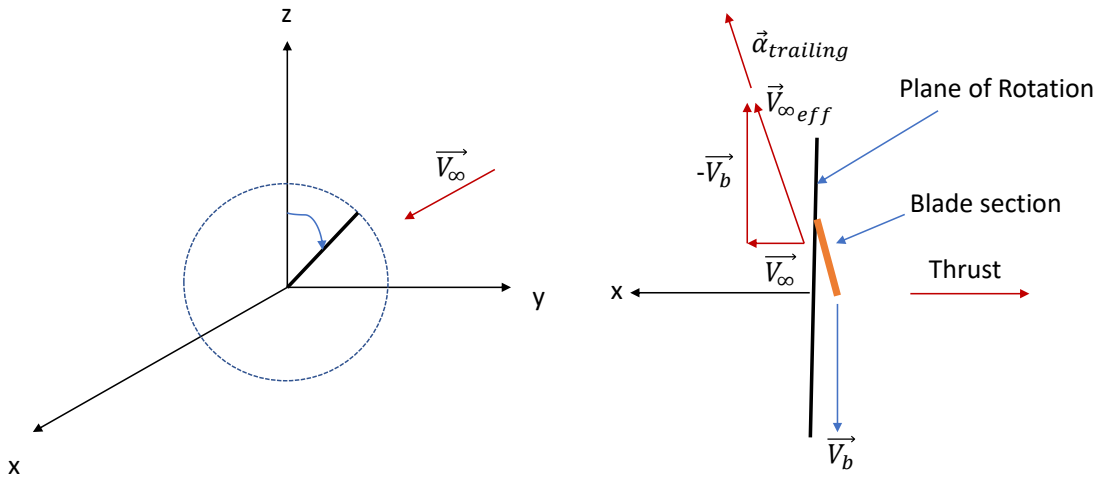

Figure 5: Propeller frame and related vectors.

the right-hand rule one can expect an upward velocity to the right of the propeller disk plane (in the $y-z$ plane) and a downwash velocity to the left of it. The distribution of upwash/downwash velocities would be the opposite if the blade twist were reversed.

3.2 Propeller Influence on a Rigid Model

Figure (6) shows the circulation of a 1-m-by-0.2-m flat plate rectangular wing placed behind a propeller located at its middle span. The propeller generates positive thrust as described by Fig. (5). Then, in accordance with the discussion above, for the propeller considered, an upwash velocity on the right portion of wing and a downwash on its left portion (looking from behind of the propeller) were expected and that is exactly what is observed in Fig. (6).

Consider the X-HALE vehicle introduced above and made rigid for this first vehicle assessment of the propeller effects. Further, consider the aircraft is flying at a uniform flow speed of 14 m/s, zero body angle of attack, no tails or aileron deflections, and the wing clamped at $y = 0$. Figure (7) shows a comparison of the wing lift distribution for the rigid X-HALE with and without propellers The result for the case with propellers was obtained using average c_l values during three periods in the 30 last time steps of a 1-second simulation (period of 0.01 s). If an average of the last 100 steps were used, the curve remains the same, indicating that it achieved a stationary average distribution. One may notice that, for this rigid case, the average distribution of c_l for the simulation with propeller was higher then the case without propeller. Also, there is a spanwise c_l oscillation with locations of maximum c_l to the right of the propeller hub positions, resulting in an overall asymmetric pattern. One can also notice an asymmetry in the local lift distribution on left and right sides of each propeller hub. This is consistence with what is described in [2]. As this propeller generates a positive thrust when it rotates in the clockwise direction with relation to axis x in Fig. (3), it generates an upwash region in the right side (positive y direction) and a downwash region in the left side of the hub, changing the local effective angle of attack on those regions.

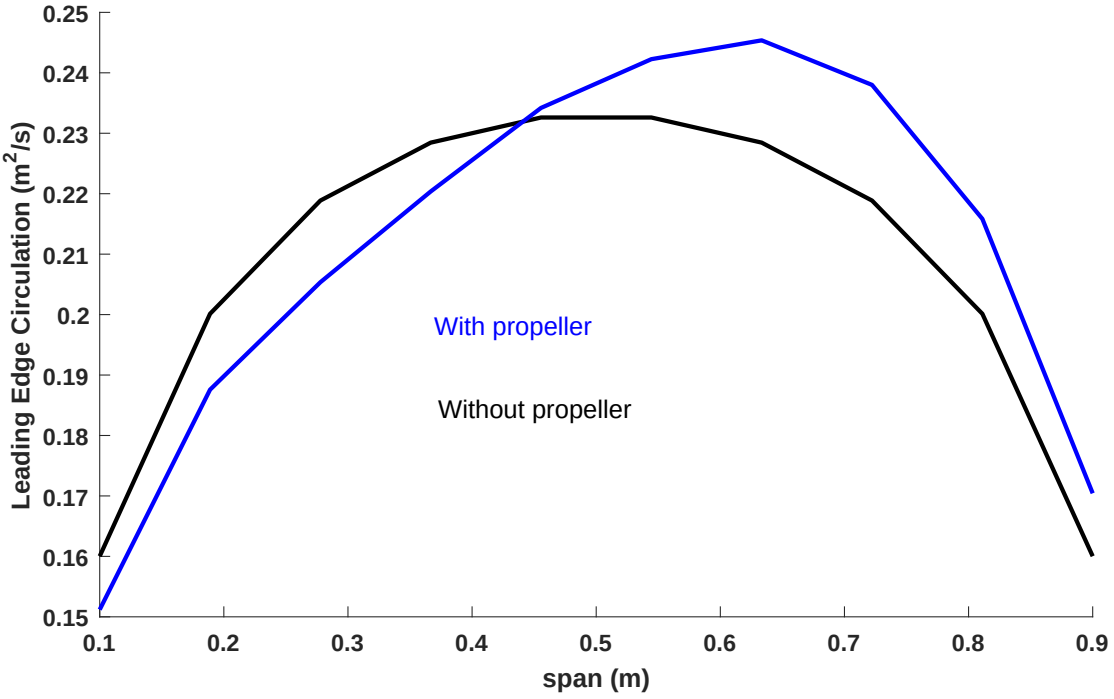

Figure 6: Span circulation distribution for a rectangular wing behind a propeller.

Consider one of the X-HALE horizontal tails located at the 2-m spanwise station (right wing), just behind one of the propellers. For this particular position the asymmetric effects of the propellers are not so noticeable on tails, but the tail lift distribution increases when the propellers are rotating, as can be observed in Fig. (8). For a flexible wing, it is expected that a change on tail lift may also change the local wing angle of attack due to the induced elastic twist.

Figure (9) shows a plot of the particles over the aircraft after 0.15 seconds of simulation. The particles are convected with the influence of the particles themselves, influence of the blades, and the surface and wake panels in such a way that they follow streamlines, avoiding problems with solid surface crossings. If one zooms near the leading edge, as shown in Fig. (10), it can be observed that the initial helicoidal pattern of the particles are modified when they interact with the wake.

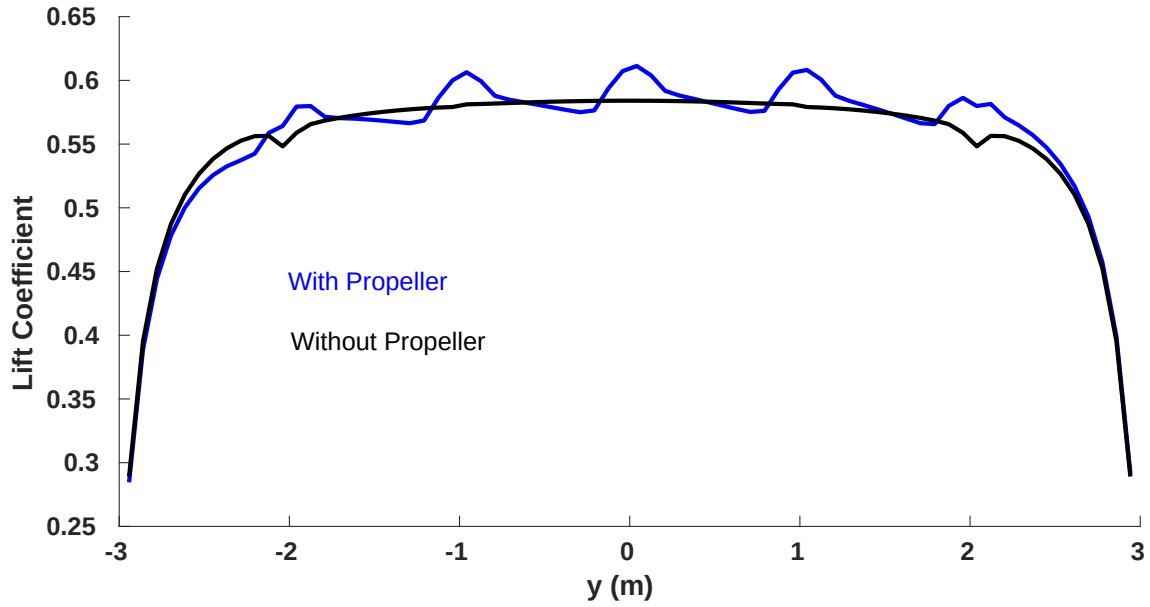

Figure 7: Distribution of c_l along wing span for rigid models with and without propellers. Average values applied for case with propellers.

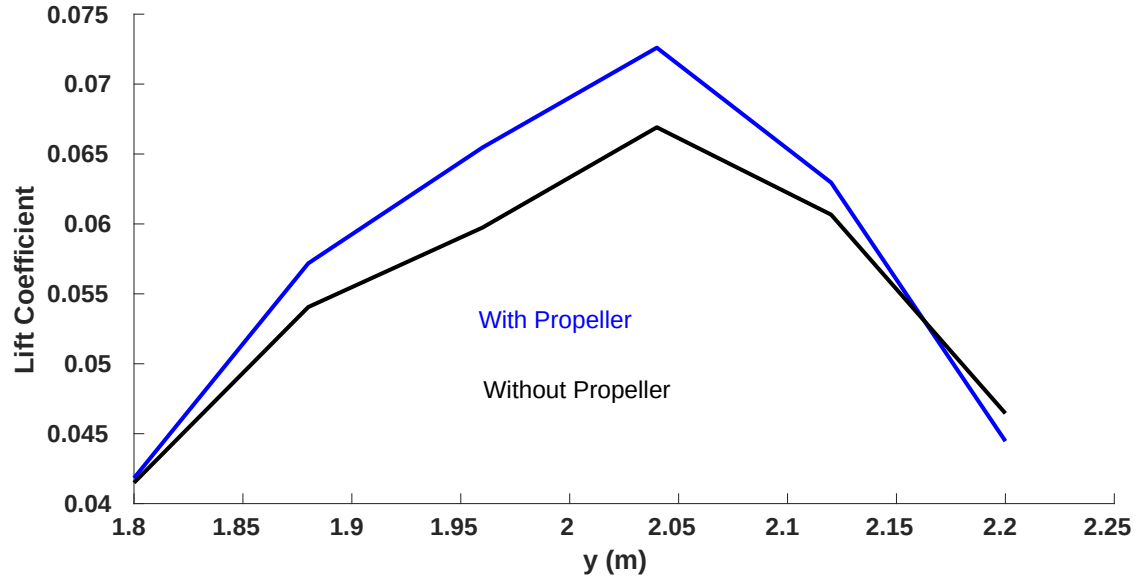

Figure 8: Distribution of c_l along tail at spanwise station $y = 2$ m for rigid models with and without propellers. Average values applied for case with propellers.

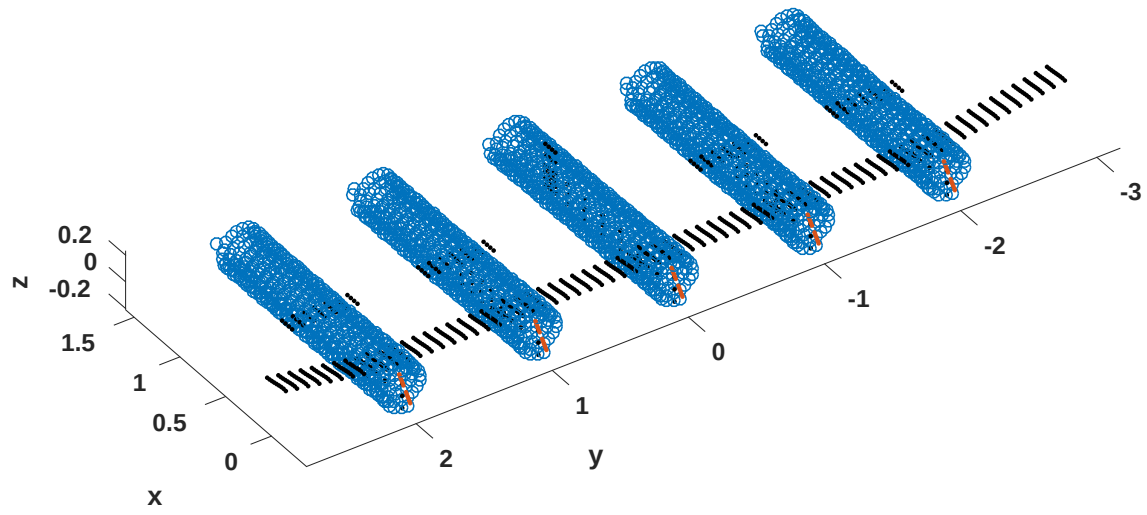

Figure 9: Vortex particles over X-HALE after 0.15 seconds of simulation with a time step of 0.0005 seconds for the propeller discretization.

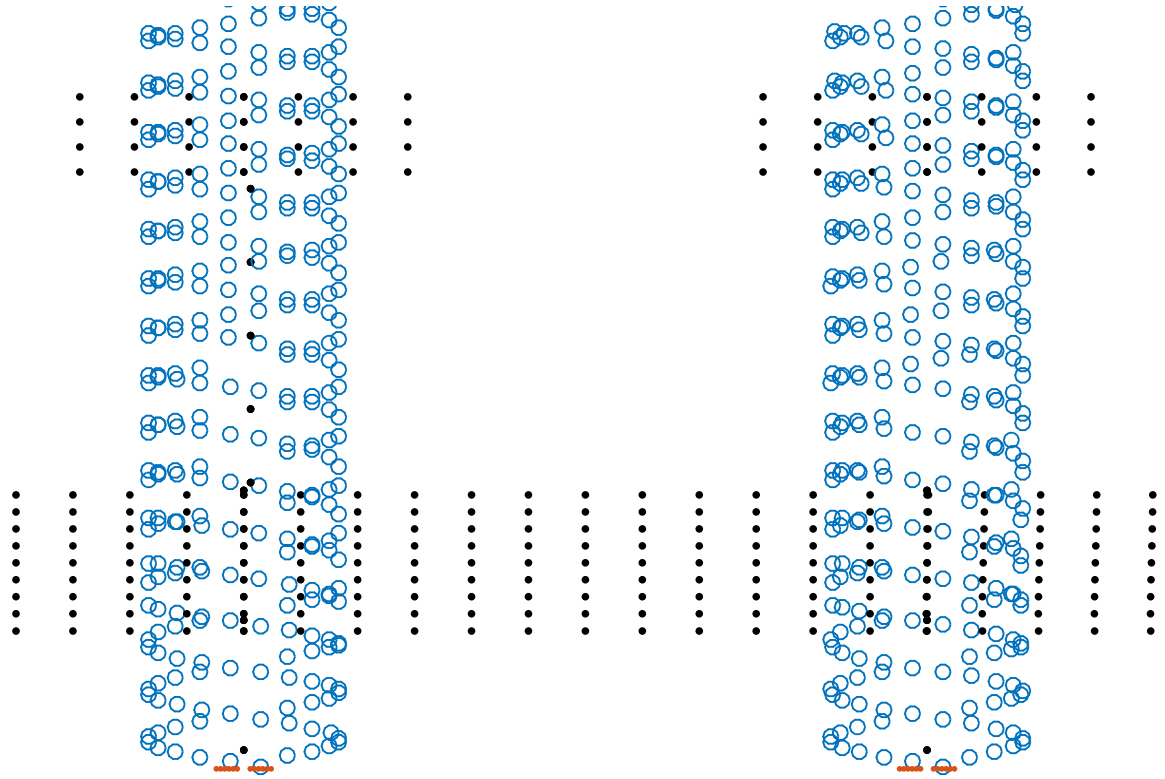

Figure 10: Zoom of particles over X-HALE for a region on the left wing.

3.3 Propeller Influence on a Flexible Model

In order to best isolate the analysis of the propeller effect and avoid, for example, the influence of the coupling motion between tail and wing, it was considered a different model for the aeroelastic simulations. The chosen model is similar to the flexible X-HALE but with only two instead of five propellers. The two propellers are located at $y = -2$ and $y = 2$ in the coordinate system showed in Fig. (3).

As one can see in Fig. (12), the distribution of lift shows a slight increase in the region near the propeller hubs. This change is lift does not have a significant effect on tip deflection, although the local increase in lift may add addition shear strength requirements on the joiner between two wing segments [19].

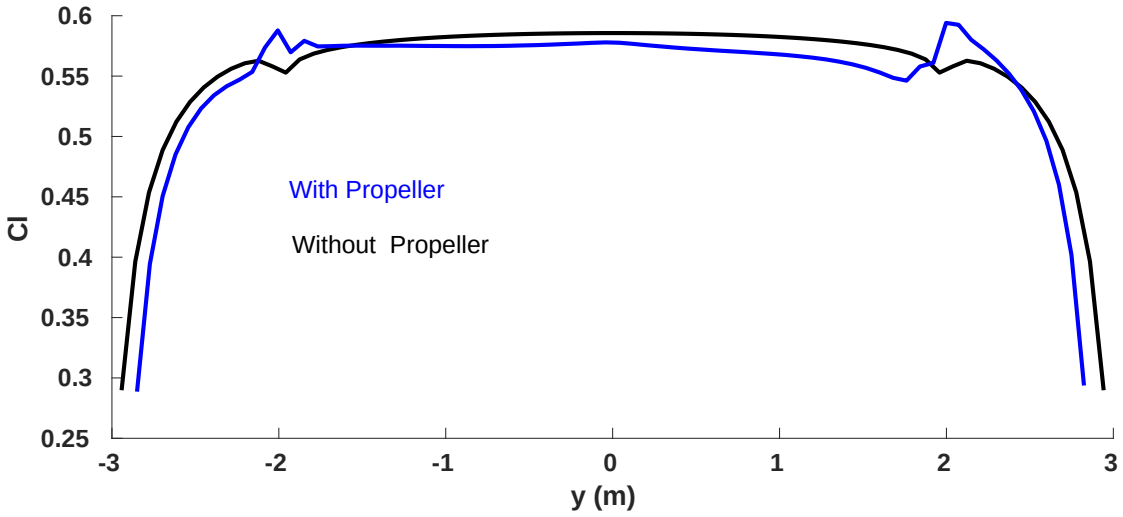

Figure 11: Lift distribution along span for equilibrium condition with and without propellers. Model is the X-HALE main wing with propellers only at spanwise stations $y = 2$ m and $y = -2$ m.

As a preliminary investigation of the dynamic response of the flexible vehicle due to control inputs, consider a symmetric aileron sinusoidal input with amplitude 5 degrees and period of 1 second. The initial equilibrium states were first obtained for the cases with and without the aerodynamic propeller effects. As shown in Fig. (12), the right wing tip deflection from the corresponding equilibrium positions shows a very similar pattern. These were expected, since the total lift with and without the propeller aerodynamic effects was kept constant (to counteract the constant weight of the vehicle). Other parameters like yaw damping should have a much more pronounced effect and will be investigated later.

4 CONCLUSIONS

In this work the propeller aerodynamic effects is modeled with the Lifting Line formulation for its blades and Viscous Vortex Particle for the slipstream. The propeller model was coupled with an Unsteady Vortex Lattice and the new aerodynamic models integrated into UM/NAST, the University of Michigan‘s nonlinear aeroelastic-coupled-flight dynamics simulation framework. For that, geometric nonlinear strain-based beam finite elements were used for the structural representation of very flexible aircraft. The enhancement pieces to UM/NAST, namely the propeller model and the uVLM for the lifting surfaces, were individually and successfully verified

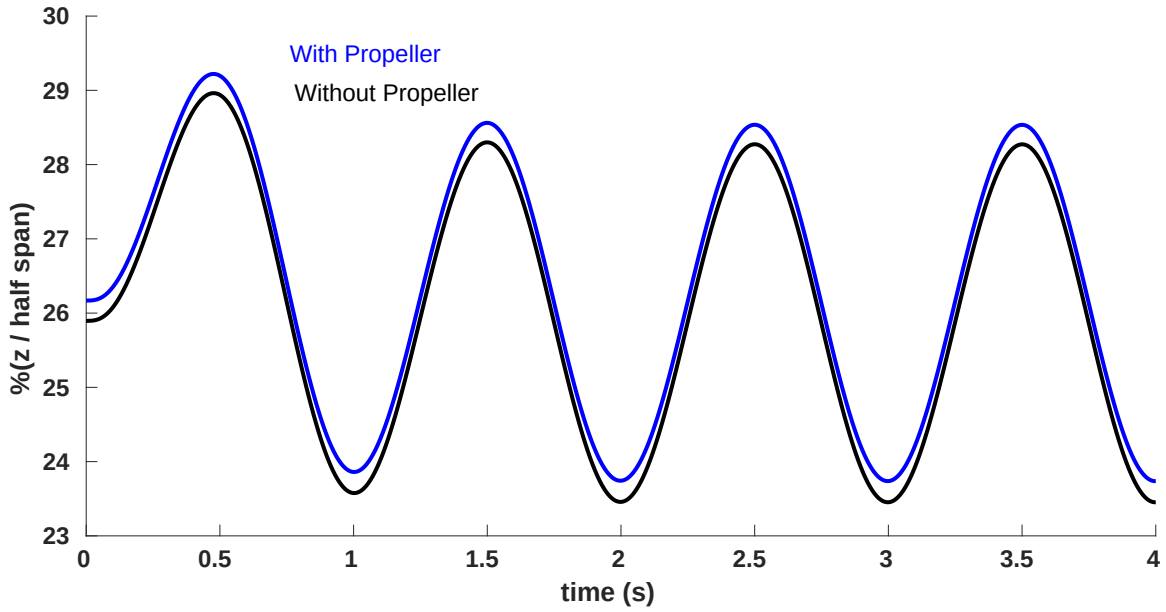

Figure 12: Right wing tip elastic deflection along the vertical plane from the trim condition in terms of percentage of half span due to symmetric aileron sinusoidal input of amplitude 5 degrees.

against other existing codes. Then the effects of the propeller wash were investigated in the X-HALE aircraft. This is a five-propeller very flexible aircraft that was developed and being tested at the University of Michigan. The preliminary results showed that the propwash affects the lift distribution over the wing, and also has an impact to the horizontal tails. More studies are warranted to assess the change in aerodynamic damping due to the present of fins and tails in the slipstream of the propellers. The particle vortex formulation showed to be a good approach to model the propeller slipstream along the aircraft surfaces, allowing a streamwise flow of particles along the wing and avoiding problems of a wake crossing a lifting surface. However optimization procedures are necessary to avoid large accumulation of particle and consequent growth in computational burden. Future work include the inclusion of the propeller dynamic effects (*e.g.,* gyroscopic effects, to complete the overall propeller modeling and the assessment of its effects on the performance and stability characteristics of a very flexible aircraft in free flight.

5 ACKNOWLEDGMENTS

The authors gratefully acknowledges the technical interactions and support from: Puneet Singh (University of Michigan) who provided comparisons with his Viscous Vortex Particle code, Cristina Riso (University of Rome La Sapienza) who provided NASTRAN-uVLM results, and Markus Ritter (DLR Institute of Aeroelasticity) who provided the uVLM code used in this work. Also, the first author gratefully acknowledges the support of CNPq (Conselho Nacional de Desenvolvimento Científico e Tecnológico, Brazil) and the University of Michigan for her academic scholarship.

6 REFERENCES

[1] Gamble, B. and Reeder, M. (2006). Experimental analysis of propeller interactions with a flexible wing micro air vehicle. In *36th AIAA Fluid Dynamics Conference and Exhibit, Fluid Dynamics and Co-located Conferences*. San Francisco, California, 5-8 June 2006. AIAA 2006-3916, 10.2514/6.2006-3916.

[2] C., A., Liu, C., Allen, C. B., Rampuravawala, A., and Ferraro, G. (2013). Propeller-flexible wing interaction using rapid computational methods. In *31st AIAA Applied Aerodynamics Conference, Fluid Dynamics and Co-located Conferences*. San Diego, California, 24-27 June 2013. AIAA 2013-2418, 10.2514/6.2013-2418.

[3] Jones, J. R. and Cesnik, C. E. S. (2015). Preliminary flight test correlations of the x-hale aeroelastic experiment. *The Aeronautical Journal*, 119(1217), 855–870.

[4] Shearer, C. M. and Cesnik, C. E. S. (2007). Nonlinear flight dynamics of very flexible aircraft. *Journal of Aircraft*, 44(5), 1528–1545.

[5] Su, W. and Cesnik, C. E. S. (2011). Dynamic response of highly flexible flying wings. *AIAA Journal*, 49(2), 324–339.

[6] Su, W. and Cesnik, C. E. S. (2010). Nonlinear aeroelasticity of a very flexible blended-wing-body aircraft. *Journal of Aircraft*, 47(5), 1539–1553.

[7] Veldhuis, L. (2005). *Propeller Wing Aerodynamic Interference*. Ph.D. thesis, Delft University of Technology, Delft.

[8] Calabretta, J. S. (2010). *A Three Dimensional Vortex Particle-panel Code for Modeling Propeller-airframe Interaction*. Master's thesis, California Polytechnic State University, San Luis Obispo.

[9] Puneet, S. and Friedman, P. P. (2017). Application of vortex methods to coaxial rotor wake and load calculations. In *AIAA Science and Technology Forum and Exposition (SciTech2017), 55th AIAA Aerospace Sciences Meeting*. Grapevine, Texas, 9-13 January 2017. AIAA 2017-0051, 10.2514/6.2017-0051.

[10] Thepvongs, S., Cesnik, C. E. S., and Voutsinas, S. G. (2005). Aeroelastic and acoustic analysis for active twist rotors. In *31st European Rotorcraft Forum*. Florence, Italy, 13-15 September 2005.

[11] He, C. and Zhao, J. (2009). Modeling rotor wake dynamics with viscous vortex particle method. *AIAA Journal*, 47(4), 902–915.

[12] Willis, D. J. (2006). *An Unsteady, Accelerated, High Order Panel Method with Vortex Particle Wakes*. Ph.D. thesis, Massachusetts Institute of Technology, Cambridge.

[13] Abedi, H., Davidson, L., and Voutsinas, S. (2013). Vortex method application for aerodynamic loads on rotor blades. In *EWEA 2013: Europe's Premier Wind Energy Event*. Vienna, Austria, 4-7 February 2013.

[14] Ritter, M., Cesnik, C. E. S., and Kruger, W. R. (2015). An enhanced modal approach for large deformation modeling of wing-like structures. In *AIAA Science and Technology Forum and Exposition (SciTech2015), 56th AIAA/ASCE/AHS/ASC Structures, Structural Dynamics, and Materials Conference*. Kissimmee, Florida, 5-9 January 2015. AIAA 2015-0176, 10.2514/6.2015-0176.

[15] Su, W. and Cesnik, C. E. S. (2011). Strain-based geometrically nonlinear beam formulation for modeling very flexible aircraft. *International Journal of Solids and Structures*, 48(16-17), 2349–2360.

[16] Winckelmans, G. S. and Leonard, A. (1993). Contributions to vortex particle methods for the computation of three-dimensional incompressible unsteady flows. *Journal of Computational Physics*, 109(2), 247–273.

[17] Brandt, J. B. (2005). *Small-scale Propeller Performance at Low Speeds*. Master's thesis, University of Illinois at Urbana-Champaign, Urbana-Champaign.

[18] Riso, C. (2016). University of Rome 'La Sapienza' - Personal Communication.

[19] Cesnik, C. E. S., Senatore, P. J., Su, W., Atkins, E. M., and Shearer, C. M. (2012). X-hale: A very flexible unmanned aerial vehicle for nonlinear aeroelastic tests. *AIAA Journal*, 50(12), 2820–2833.

[20] Ritter, M., Jones, J., and Cesnik, C. E. S. (2016). Enhanced modal approach for free-flight nonlinear aeroelastic simulation of very flexible aircraft. In *AIAA Science and Technology Forum and Exposition (SciTech2016), 15th Dynamics Specialists Conference*. San Diego, California, 4-8 January 2016. AIAA 2016-1794, 10.2514/6.2016-1794.

COPYRIGHT STATEMENT